Available online at www.sciencedirect.com
SCIENCE DIRECT®
Tectonophysics 376 (2003) 185–197
TECTONOPHYSICS
www.elsevier.com/locate/tecto

Comparison between thermal–viscous coupling and frictional sliding

Masanori Kameyama*

Research Program of Plate Dynamics, Institute for Frontier Research on Earth Evolution (IFREE), Japan Marine Science and Technology Center (JAMSTEC), Japan

Received 5 March 2002; accepted 29 September 2003

Abstract

We investigated the similarity between thermal–viscous coupling (TVC) and frictional sliding, proposed by Kameyama and Kaneda [Pure Appl. Geophys. 159 (2002) 2011]. We consider a one-dimensional layer composed of viscous material, which is sandwiched and sheared by two thick elastic layers. The rate of viscous deformation depends on the temperature T_c in the viscous layer as well as shear stress τ. The temperature T_c changes owing to heating by viscous dissipation and conductive cooling. We carried out velocity-stepping tests for the steady-state deformation both numerically and analytically, and compared the temporal evolution of small perturbations with that of the spring-block model with rate- and state-dependent friction (RSF). We found that, as is the case of frictional slip stability, the manner of temporal evolution is classified into four regimes depending on whether it is stable or not and whether it is monotonous or oscillatory with time. By further interpreting TVC in terms of general RSF theory by Ruina [J. Geophys. Res. 88 (1983) 10359], we obtained the relations between the parameters appearing in the phenomenological RSF law and the nondimensional parameters which characterize the nature of TVC. A further improvement of this approach might be important for estimating the actual values of frictional constitutive parameters at the deeper portion of seismogenic faults of interplate or inland earthquakes where a ductile deformation is expected to be significant.

Keywords: Friction law; Viscous dissipation; Viscoelasticity; Shear instability; Earthquakes

1. Introduction

A constitutive relationship of faults, which relates the fault slip, applied stress, and other geophysical ambient conditions, is one of the most important factors in the study of earthquake occurrence. Understanding the constitutive relationship enables us to estimate where and under which conditions unstable (i.e. seismogenic) fault slip takes place. In these decades, several realistic models of rock friction have been proposed on the basis of laboratory experiments. In particular, the rate- and state-dependent friction law (e.g. Dieterich, 1979; Ruina, 1983) has been commonly employed both in interpreting the experimental results of rock friction (e.g. Blanpied et al., 1998) and

* Present address: Computational Earth Science Research Program, Earth Simulator Center, Japan Marine Science and Technology Center, 3173-25 Showa-machi, Kanazawa, Yokohama, Kanagawa 236-0001, Japan. Tel.: +81-45-778-5886; fax: +81-45-778-5493.

E-mail address: kameyama@jamstec.go.jp (M. Kameyama).

0040-1951/$ - see front matter © 2003 Elsevier B.V. All rights reserved.
doi:10.1016/j.tecto.2003.09.012

in numerical modeling of fault slip (e.g. Rice, 1993). Earlier numerical studies of earthquake generation (e.g. Tse and Rice, 1986; Stuart, 1988; Kato and Hirasawa, 1997; Kuroki et al., 2002) have demonstrated that this friction law reproduces many geophysical phenomena such as earthquake cycles and related crustal deformation.

The uncertainty in the numerical modeling of earthquake cycles, however, lies in estimating the constitutive parameters along the modeled faults or plate boundaries, especially those at depth. In most of earlier numerical models (Tse and Rice, 1986; Stuart, 1988; Kato and Hirasawa, 1997; Kuroki et al., 2002), the values of the constitutive parameters have been assumed a priori, either by extrapolating from laboratory experiments or by assuming a seismogenic condition at a desired range of depth. This is because the values of parameters in the deeper portion of earthquakes faults are not well constrained. Since it is difficult to conduct friction experiments of rocks under the conditions for deep earthquake faults, it is required to get deep physical insights into rock friction theoretically in order to estimate the values of constitutive parameters in the real faults or plate boundaries and, hence, to further improve the models of earthquake occurrence.

On the other hand, recent work by Kameyama and Kaneda (2002) demonstrated that a shear deformation of viscoelastic material bears a feature quite similar to that of frictional slip with the help of thermal–viscous coupling (hereafter denoted by TVC); namely an interaction between temperature-dependence of viscosity and temperature rise due to viscous dissipation. In this paper, we extend the work of Kameyama and Kaneda (2002) and investigate the similarity between TVC and the rate- and state-dependent friction (hereafter denoted by RSF). In Section 2, we briefly review the nature of the friction law. In Section 3, we develop the idea of TVC. By comparing the behavior of TVC with that of RSF, we then discuss the properties of TVC from a viewpoint of a general class of RSF. In the earlier studies of TVC (Hobbs and Ord, 1988; Ogawa, 1987), its application to earthquake occurrence has been limited to that of intermediate and/or deep-focus earthquakes within subducting slabs. In this study, in contrast, we seek for an applicability of TVC to the earthquake occurrence in the shallow portion of the Earth, such as interplate or inland earthquakes, through the comparison between TVC and RSF.

2. Nature of rate- and state-dependent friction law

In this section, we briefly review the nature of RSF. There are several versions of this friction law (see Marone, 1998; Scholz, 1998 for a review). According to Ruina (1983), the RSF should follow two general assumptions (hereafter denoted by GRSF); (i) the friction depends on the slip rate V and the state of the slip surface represented by the state variable Θ, and (ii) the temporal evolution of state depends also on V and Θ. That is,

$$\begin{cases} \mu = F_{\mathrm{rsf}(V,\Theta),} \\ \dfrac{\mathrm{d}\Theta}{\mathrm{d}t} = G_{\mathrm{rsf}(V,\Theta).} \end{cases} \tag{1}$$

Here μ is the friction coefficient, and we ignored the dependence on normal force N for simplicity.

We study the stability of steady-state slip of GRSF using a spring-block model, which is schematically illustrated in Fig. 1. Here we assume a quasi-static motion of block for simplicity and, hence, ignore the effect of inertia, which may affect a dynamic behavior of the model (Rice and Tse, 1986). According to the

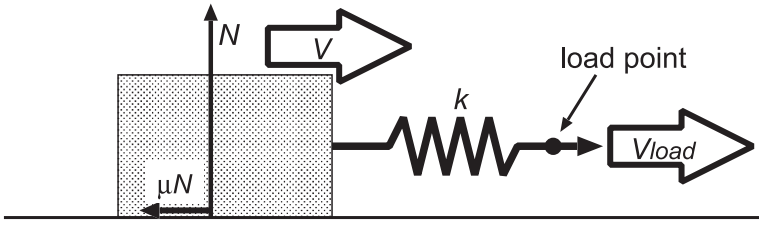

Fig. 1. Schematic cartoon of spring-block model.

linear stability analysis by Ruina (1983), a growth rate λ of infinitesimal perturbations of the state variable, friction coefficient, and slip velocity (denoted by $\delta\Theta$, $\delta\mu$, and δV, respectively) is determined by the following quadratic equation,

$$\lambda^2 - (\beta - \gamma - 1)\omega\lambda + \omega^2\gamma = 0. \tag{2}$$

In Eq. (2), we introduced three parameters ω, β and γ defined by,

$$\omega = -G_{\mathrm{rsf},\Theta}, \tag{3}$$

$$\beta = \frac{F_{\mathrm{rsf},\Theta}}{F_{\mathrm{rsf},V}}\frac{G_{\mathrm{rsf},V}}{G_{\mathrm{rsf},\Theta}}, \tag{4}$$

$$\gamma = -\frac{k/N}{F_{\mathrm{rsf},V}G_{\mathrm{rsf},\Theta}}, \tag{5}$$

where the commas in subscripts indicate partial differentiation, k is the spring constant, V_s is the slip velocity of the block for a steady state, and N is the normal force acting on the block. Eq. (3) comes from the fact that $-G_{\mathrm{rsf},\Theta}$ corresponds to the healing rate of $\delta\Theta$ (note that $\mathrm{d}(\delta\Theta)/\mathrm{d}t = G_{\mathrm{rsf},V}\delta V + G_{\mathrm{rsf},\Theta}\delta\Theta$) and, in other words, acts as an intrinsic evolution rate of the system. From Eqs. (4) and (5), we can understand the meanings of β and γ as follows. The parameter β represents the ratio of the rate of decrease in $\delta\mu$ due to δV through the change in $\delta\Theta$ ($=-F_{\mathrm{rsf},\Theta}G_{\mathrm{rsf},V}\,\delta V$) to the rate of increase in $\delta\mu$ directly coming from δV ($=\omega F_{\mathrm{rsf},V}\,\delta V$). The parameter γ, on the other hand, represents the ratio of the rate of elastic loading by δV ($=k\delta V$) to the rate of increase in frictional resistance directly coming from δV ($=\omega N F_{\mathrm{rsf},V}\,\delta V$).

To describe in detail the conditions of slip stability obtained above, we assume in the following a phenomenological form of this friction law (hereafter denoted by "laboratory-derived RSF", or LRSF). For example, we employ "Ruina–Dieterich" or "slip" law (e.g. Ben-Zion and Rice, 1995), which has been widely employed in numerical modeling of fault slip (e.g. Rice, 1993). This friction law is given by the two equations,

$$\begin{cases} \mu = \mu_o + \Theta + a\ln\left(\dfrac{V}{V_c}\right), \\ \dfrac{\mathrm{d}\Theta}{\mathrm{d}t} = -\dfrac{V}{d_c}\left[\Theta + b\ln\left(\dfrac{V}{V_c}\right)\right]. \end{cases} \tag{6}$$

Here d_c is the characteristic slip length, and μ_o and V_c are constants. In particular, the parameters a and b determine whether steady-state sliding is potentially stable or not to a velocity perturbation, and d_c represents the length scale over which the evolution of μ occurs through the evolution of Θ during a slip. In this case, the paramters ω, β, and γ can be written as,

$$\omega = \frac{V_o}{d_c}, \beta = \frac{b}{a}, \gamma = \frac{kd_c}{Na}, \tag{7}$$

where V_o is the slip velocity at the steady state.

To see how the evolution of infinitesimal perturbations differs depending these parameters, we solve Eq. (2) for the growth rate λ. Here we define the functions A_{rsf} and D_{rsf} as

$$A_{\mathrm{rsf}}(\beta,\gamma) \equiv \frac{1}{2}(\beta - \gamma - 1), \tag{8}$$

$$D_{\mathrm{rsf}}(\beta,\gamma) \equiv \frac{1}{4}(\beta - \gamma - 1)^2 - \gamma, \tag{9}$$

so that the solution λ can be written as $\lambda = (A_{\mathrm{rsf}} \pm \sqrt{D_{\mathrm{rsf}}})\omega$. Fig. 2 shows the variations in A_{rsf} and D_{rsf} depending on β and γ. The solid line divides the β–γ plane into the regime with $A_{\mathrm{rsf}}>0$ (indicated by the letter "U") and that with $A_{\mathrm{rsf}}<0$ (indicated by the letter "S"). The dashed line, on the other hand, divides the β–γ plane into the regime with $D_{\mathrm{rsf}}>0$ (indicated by S1 and U1) and that with $D_{\mathrm{rsf}}<0$ (indicated by S2 and U2). As can be seen from the figure, the β–γ plane is divided into four regimes by the two lines, namely the regimes U1 ($A_{\mathrm{rsf}}>0, D_{\mathrm{rsf}}>0$), U2 ($A_{\mathrm{rsf}}>0, D_{\mathrm{rsf}}<0$), S1 ($A_{\mathrm{rsf}}<0, D_{\mathrm{rsf}}>0$), and S2 ($A_{\mathrm{rsf}}<0, D_{\mathrm{rsf}}<0$).

Fig. 2 implies that the response of steady state to an infinitesimal perturbation differs between the regimes owing to the difference in the sign of A_{rsf} and D_{rsf}. The sign of A_{rsf} classifies the stability of steady state to an infinitesimal perturbation; the steady state becomes unstable in the regimes U1 and U2 ($A_{\mathrm{rsf}}>0$), while it becomes stable in the regimes S1 and S2 ($A_{\mathrm{rsf}}<0$). In addition, the sign of D_{rsf} classifies the type of temporal evolution of the perturbation; the temporal evolution occurs monotonously in regimes S1 and U1 ($D_{\mathrm{rsf}}>0$), while it takes place in an

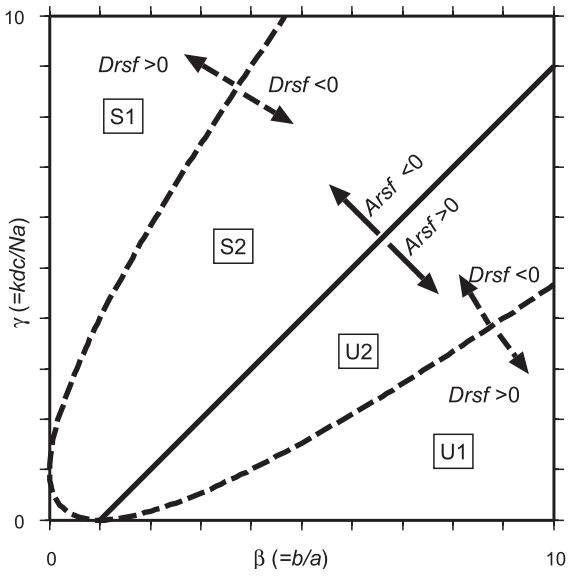

Fig. 2. Regime diagram for the variation in the growth rate λ of infinitesimal perturbation depending on the changes in β and γ obtained for the spring-block model with rate- and state-dependent friction law. The solid and dashed lines indicate the plots of $A_{rsf}=0$ and $D_{rsf}=0$, respectively. See the text as for the definitions of the labels "U1", "U2", "S1", and "S2".

oscillatory manner in the regimes S2 and U2 ($D_{rsf}<0$). We confirmed that the above classification is valid by comparing the numerical results of the evolution of finite-amplitude perturbation conducted by Ruina (1983).

Fig. 2 also shows that the regimes for an unstable evolution take place only when $\beta>1$ and $\gamma<\beta-1$. This is consistent with the earlier results of frictional slip stability that steady-state sliding is unstable only when $a-b<0$ and the spring constant k is smaller than a threshold value $k_c=(b-a)N/d_c$ (Ruina, 1983).

3. Nature of thermal–viscous coupling

In this section, we discuss the nature of TVC by using a one-dimensional model of shear deformation similar to those employed in Ogawa (1987) and Kameyama and Kaneda (2002). First we introduce the conceptual model and fundamental equations. Next we carry out velocity-stepping tests both numerically and analytically, to reveal a similarity of TVC with the frictional behavior obtained in Section 2. We then investigate the similarity between TVC and RSF by interpreting TVC in terms of GRSF.

3.1. Model description

In Fig. 3, we schematically show the conceptual model employed here. We consider shear deformation of a viscous material with an infinite Prandtl number in a layer of half-width h placed between two elastic layers of thickness L. The inner viscous layer and outer elastic layers correspond to the frictional surface and the spring for the spring-block model, respectively. (Or, if we regard the present model as an actual fault, the inner and outer layers can be regarded as a fault zone and host rocks, respectively.) The viscosity of material in the inner layer is assumed to depend both on stress τ and temperature T. The z-axis is chosen to run across the layers, and the center and outer boundaries are chosen to be $z=0$ and $z=\pm(L+h)$, respectively. The material moves in the x-direction with a constant velocity $\pm V_w$ at the outer boundaries $z=\pm(L+h)$, respectively. The temperature is assumed to be T_c and T_w in the inner and outer layers, respectively. The assumption for temperature-distribution comes from a simplification of the steady-state temperature-distribution obtained by one-dimensional numerical calculations (Kameyama and Kaneda, 2002), and similar to that employed in the "heterogeneous model" of Ogawa (1987).

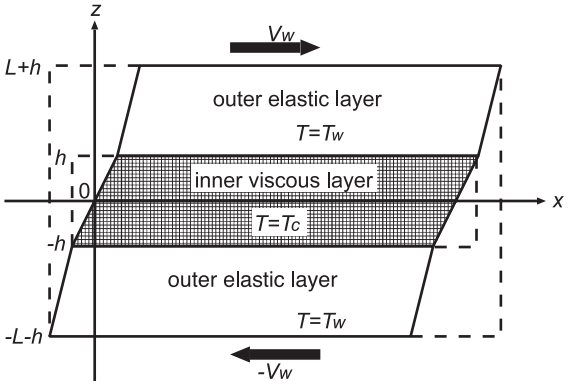

Fig. 3. Schematic illustration of conceptual model employed in this study.

The motion of the material in the layer is given by,

$$2V_{\mathrm{w}} = 2h\dot{\varepsilon}_{\mathrm{v}(\tau,T=T_{\mathrm{c}})} + 2L\frac{1}{G}\frac{\mathrm{d}\tau}{\mathrm{d}t}, \tag{10}$$

where $\dot{\varepsilon}_v$ is the strain rate due to viscous deformation in the inner layer, and G is the shear modulus or rigidity in the outer layers. Here we assumed that the shear stress τ is constant in the inner and outer layers. Eq. (10) can be further simplified as,

$$2V_{\mathrm{w}} = 2h\left[\dot{\varepsilon}_{\mathrm{v}(\tau,T=T_{\mathrm{c}})} + \frac{1}{G_{\mathrm{eff}}}\frac{\mathrm{d}\tau}{\mathrm{d}t}\right], \tag{11}$$

where $G_{\mathrm{eff}} \equiv (h/L)G$ is an "apparent" or "effective" rigidity. Eq. (11) means that the deformation of the entire layer is mathematically equivalent to that of a layer of half-thickness h composed of a Maxwell viscoelastic material whose rigidity is G_{eff}.

We assume that the equation for the change in the temperature T_{c} in the inner viscous layer is given by,

$$\rho C_{\mathrm{p}}(2h)\frac{\mathrm{d}T_{\mathrm{c}}}{\mathrm{d}t} = -2\rho C_{\mathrm{p}}\kappa\frac{T_{\mathrm{c}} - T_{\mathrm{w}}}{h} + \tau\dot{\varepsilon}_{\mathrm{v}(\tau,T_{\mathrm{c}})}(2h), \tag{12}$$

where ρC_{p} is the volumetric heat capacity, and κ is the thermal diffusivity. In Eq. (12), the left-hand term represents the rate of change in the thermal (internal) energy in the viscous layer, the first term in the right-hand side represents the conductive heat flux flowing out of the layer across the layer interfaces ($z = \pm h$), and the second term represents the rate of heating by viscous dissipation in the layer. Here we assumed that the temperature in the outer layers T_{w} is constant. This implies that the timescale of thermal conduction over the inner layer is much longer than that considered here.

3.2. Velocity-stepping test for thermal–viscous coupling

In this subsection, we carry out velocity-stepping tests to demonstrate the behavior of TVC. In particular, we focus on the differences in the temporal evolution due to the difference in G_{eff}, to compare well with the behavior of the spring-block model (Fig. 1) with LRSF.

We consider the temporal evolution in τ and T_{c} when a steady-state solution for $V_{\mathrm{w}} = V_{\mathrm{wo}} = \kappa/h$ is perturbed by a sudden velocity step $\delta V_{\mathrm{w}} = 0.1 V_{\mathrm{wo}}$ at time $t = 0$. In the following analysis, the material properties are taken to be close to those of olivine. In addition, the viscous deformation takes place by the power-law creep described by,

$$\dot{\varepsilon}_{\mathrm{v}(\tau,T)} = A_n\tau^n exp\left(-\frac{E_n}{RT}\right). \tag{13}$$

In Eq. (13), all of the constants are chosen to give a strain rate close to that associated with dislocation creep of dry olivine (Karato et al., 1986; Kameyama et al., 1999). The adopted values of parameters are summarized in Table 1. We carried out numerical calculations for various values of L, to see how the variation in the rigidity G_{eff} affects the temporal evolution of perturbations.

In Fig. 4, we show the temporal evolution of τ and T_{c} in response to the velocity step at $t = 0$ for several cases listed in Table 2. There are four types of the temporal evolution of perturbations. In Case 1 where G_{eff} is the largest, the stress τ increases very rapidly during a short period around $t = 0$ in response to the step change in V_{w}, and then gradually decreases to the value for the new steady state during the subsequent period of $t < 10h^2/\kappa$. The temperature T_{c} gradually increases to the new steady-state value during $0 < t < 10h^2/\kappa$. In Case 2, the temporal evolution of both τ and T_{c} is characterized by a decaying oscillation which evolves toward the new steady state. In Case 3, both τ and T_{c} oscillate with time in response to the velocity step. However, the amplitude of the oscillation grows with time and, neither τ nor T_{c} reaches new

Table 1
Values of physical parameters adopted in the numerical calculations presented in Figs. 4, 5 and 6

Symbol	Description	Value
G	rigidity in outer layers	8×10^{10} Pa
h	half-thickness of inner layer	10^5 m
ρC_{p}	volumetric heat capacity	2.4×10^6 J/m^3 K
κ	thermal diffusivity	10^{-6} m^2/s
A_n	pre-exponential constant	3.24×10^{-16} Pa^{-n} s^{-1}
n	stress index	3.5
E_n	activation energy	5.4×10^5 J/mol K
R	universal gas constant	8.31 J/mol K
T_{w}	temperature in elastic layers	900 K

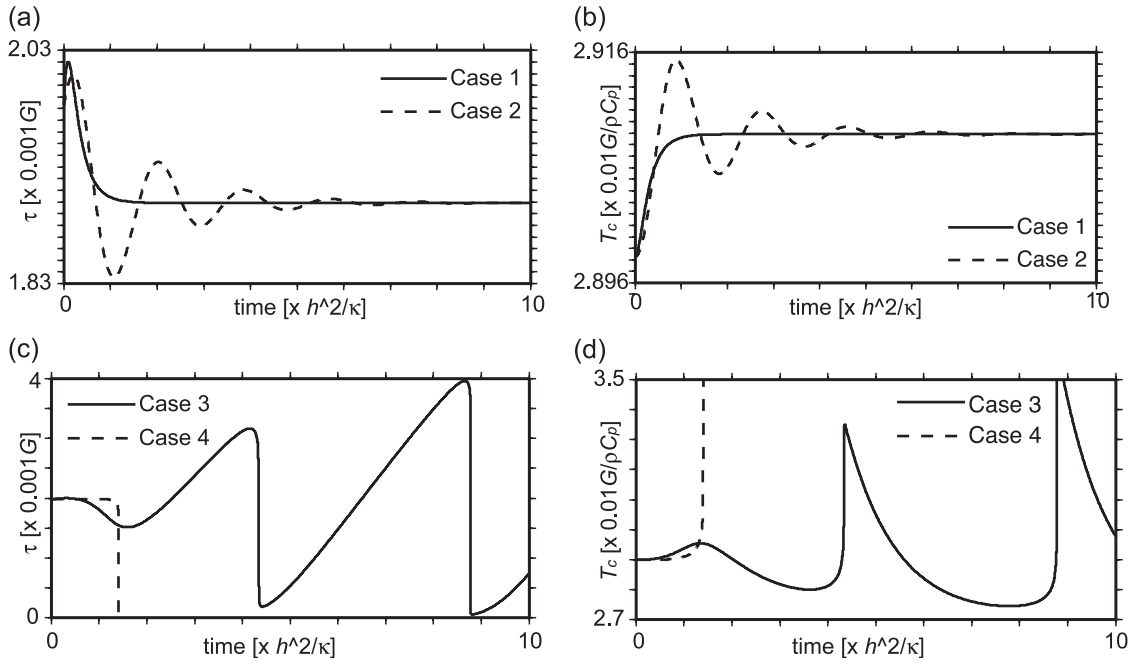

Fig. 4. Temporal evolution of shear stress τ and temperature T_c in the viscous layer for the cases of stable evolution (a and b) and unstable evolution (c and d). The units of stress and temperature are $G=8\times10^{10}$ Pa and $G/\rho C_p=3.33\times10^4$ K, respectively.

steady-state values. In Case 4 where G_{eff} is the smallest, both τ and T_c gradually increase at a much lower rate than in other cases for $t>0$ and, instead of reaching the new steady state, a sudden drop in τ and an explosive increase in T_c occur at $t\sim1.4h^2/\kappa$.

By comparing these results and those in Section 2, we notice that the four types of the temporal evolution of perturbations for TVC are the same as those obtained from the linear analysis for GRSF. Thus, we can conclude that TVC behaves quite similarly to that of LRSF.

Table 2
The values of $h/L(=G_{eff}/G)$ adopted in the numerical calculations presented in Fig. 4. Also shown are the values of nondimensional parameters f and g for initial states, and the type of temporal evolution of $\delta\tau$ and δT_c estimated from f and g

Case	$h/L(=G_{eff}/G)$	g	f	Type
1	1.0×10^{-2}	5.302	17.652	S1
2	2.5×10^{-3}	5.302	4.413	S2
3	1.0×10^{-3}	5.302	1.7652	U2
4	1.0×10^{-4}	5.302	0.17652	U1

3.3. Linear analysis of velocity-stepping test

In this subsection, we conduct a linear analysis of the steady-state solution of Eqs. (11) and (12) to study the behavior of the model in detail. In particular, we discuss which quantities determine the type of temporal evolution of perturbations in response to a velocity step.

Suppose that the temperature T_c changes from T_s to $T_s+\delta T_c$, and stress τ changes from τ_s to $\tau_s+\delta\tau$ when the velocity V_w slightly increases from V_{wo} to $V_{wo}+\delta V_w$. Here, T_s and τ_s are the steady-state solution and δT_c and $\delta\tau$ are perturbations. By substituting the above equations into Eqs. (11) and (12), we obtain the equations for steady-state values as well as the linearized equations for perturbations δT_c and $\delta\tau$. The equations for steady-state values are,

$$0=G_{eff}\left(\frac{V_{wo}}{h}-\dot{\varepsilon}_s\right), \tag{14}$$

$$0=-\frac{\kappa}{h^2}(T_s-T_w)+\frac{1}{\rho C_p}\tau_s\dot{\varepsilon}_s, \tag{15}$$

and the linearized equations for perturbations $\delta\tau$ and δT_c are,

$$\frac{d}{dt}\delta\tau = -G_{eff}\left(\frac{\partial\dot{\varepsilon}_v}{\partial\tau}\right)_{(\tau_s,T_s)}\delta\tau - G_{eff}\left(\frac{\partial\dot{\varepsilon}_v}{\partial T}\right)_{(\tau_s,T_s)}\delta T_c + \frac{G_{eff}}{h}\delta V_w, \tag{16}$$

$$\frac{d}{dt}\delta T_c = \frac{1}{\rho C_p}\left[\tau_s\left(\frac{\partial\dot{\varepsilon}_v}{\partial\tau}\right)_{(\tau_s,T_s)} + \dot{\varepsilon}_s\right]\delta\tau + \left[\frac{\tau_s}{\rho C_p}\left(\frac{\partial\dot{\varepsilon}_v}{\partial T}\right)_{(\tau_s,T_s)} - \frac{\kappa}{h^2}\right]\delta T_c. \tag{17}$$

Here we introduce three nondimensional parameters f, g, and n defined by,

$$f \equiv \frac{h^2}{\kappa}G_{eff}\left(\frac{\partial\dot{\varepsilon}_v}{\partial\tau}\right)_{(\tau_s,T_s)}, \tag{18}$$

$$g \equiv \frac{h^2}{\kappa}\frac{\tau_s}{\rho C_p}\left(\frac{\partial\dot{\varepsilon}_v}{\partial\tau}\right)_{(\tau_s,T_s)}, \tag{19}$$

$$n \equiv \frac{\tau_s}{\dot{\varepsilon}_s}\left(\frac{\partial\dot{\varepsilon}_v}{\partial\tau}\right)_{(\tau_s,T_s)}, \tag{20}$$

respectively. The parameter n is an index of the stress-dependence of the rate of viscous deformation, and equivalent to n in Eq. (13). The physical meanings of f and g will be discussed in detail in Section 3.4. By using f, g, and n, Eqs. (16) and (17) can be written as,

$$\frac{h^2}{\kappa}\frac{d}{dt}(\delta\tau) = -f\delta\tau - \rho C_p\frac{G_{eff}}{\tau_s}g\delta T_c + \frac{hG_{eff}}{\kappa}\delta V_w, \tag{21}$$

$$\frac{h^2}{\kappa}\frac{d}{dt}(\delta T_c) = \frac{1}{\rho C_p}\frac{\tau_s}{G_{eff}}f\left(1+\frac{1}{n}\right)\delta\tau + (g-1)\delta T_c. \tag{22}$$

The solution of Eqs. (21) and (22) is given by,

$$\begin{aligned}\delta\tau = {} & \frac{hG_{eff}}{\kappa}\delta V_w\frac{1-g}{f(1+g/n)} + \frac{hG_{eff}}{\kappa}\delta V_w\frac{1}{\lambda_2-\lambda_1} \\ & \times\left[\frac{\kappa}{h^2}+\lambda_2\frac{1-g}{f(1+g/n)}\right]\exp(\lambda_1 t) \\ & -\frac{hG_{eff}}{\kappa}\delta V_w\frac{1}{\lambda_2-\lambda_1} \\ & \times\left[\frac{\kappa}{h^2}+\lambda_1\frac{1-g}{f(1+g/n)}\right]\exp(\lambda_2 t),\end{aligned} \tag{23}$$

$$\begin{aligned}\delta T_c = {} & \frac{h\tau_s}{\rho C_p\kappa}\delta V_w\frac{1+1/n}{1+g/n} \\ & -\frac{h\tau_s}{\rho C_p\kappa}\delta V_w\frac{1}{\lambda_2-\lambda_1}\frac{f+\lambda_1}{g} \\ & \times\left[\frac{\kappa}{h^2}+\lambda_2\frac{1-g}{f(1+g/n)}\right]\exp(\lambda_1 t) \\ & +\frac{h\tau_s}{\rho C_p\kappa}\delta V_w\frac{1}{\lambda_2-\lambda_1}\frac{f+\lambda_2}{g} \\ & \times\left[\frac{\kappa}{h^2}+\lambda_1\frac{1-g}{f(1+g/n)}\right]\exp(\lambda_2 t),\end{aligned} \tag{24}$$

where λ_1 and λ_2 are the roots of the quadratic equation

$$\lambda^2 - (g-f-1)\frac{\kappa}{h^2}\lambda + f\left(1+\frac{g}{n}\right)\left(\frac{\kappa}{h^2}\right)^2 = 0. \tag{25}$$

(In obtaining Eqs. (23) and (24), we assumed that $\lambda_1 \neq \lambda_2$.)

To see the temporal evolution of perturbations, we solve Eq. (25) and study the nature of λ. Here we define two functions A_{tvc} and D_{tvc} as,

$$A_{tvc}(f,g) \equiv \frac{1}{2}(g-f-1), \tag{26}$$

$$D_{tvc}(f,g,n) \equiv \frac{1}{4}(g-f-1)^2 - f\left(1+\frac{g}{n}\right), \tag{27}$$

so as to write the solution of Eq. (25) as $\lambda = (A_{tvc} \pm \sqrt{D_{tvc}})(\kappa/h^2)$.

We show in Fig. 5 the plots of $A_{tvc}(f, g) = 0$ and $D_{tvc}(f, g, n) = 0$ by solid and dashed lines, respectively. We assumed $n = 3.5$, the value obtained for the deformation of dry olivine due to dislocation creep (Karato et al., 1986). The meanings of the labels in

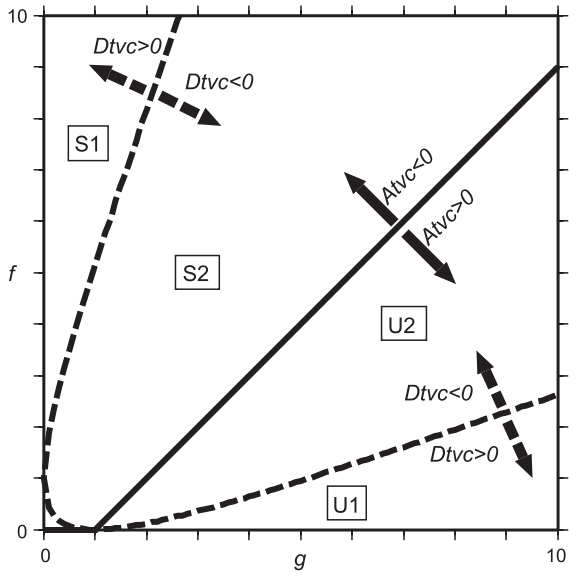

Fig. 5. Regime diagram for the variation in the growth rate λ of infinitesimal perturbation depending on the changes in f and g. The solid and dashed lines indicate the plots of $A_{\mathrm{tvc}}=0$ and $D_{\mathrm{tvc}}=0$, respectively. The employed value of n is 3.5. See the text as for the definitions of "U1", "U2", "S1", and "S2".

Fig. 5 are the same as those in Fig. 2. From the same reason as in Fig. 2, the steady state becomes unstable in the regimes U1 and U2 where $A_{\mathrm{tvc}}>0$, while it becomes stable in the regimes S1 and S2 where $A_{\mathrm{tvc}}<0$. In addition, the temporal evolution of perturbation occurs monotonously in regimes S1 and U1 where $D_{\mathrm{tvc}}>0$, while it takes place in an oscillatory manner in the regimes S2 and U2 where $D_{\mathrm{tvc}}<0$.

We now apply the above classification of solution to the numerical results presented in Fig. 4. In Table 2, we also show the values of nondimensional parameters f and g for the initial state of the calculations (i.e. steady state for $V_{\mathrm{w}}=V_{\mathrm{wo}}$) and the class of solutions expected from the values of f and g. From Table 2 and Fig. 4 we can conclude that the classification from the linear analysis is valid for the numerical calculations presented in Fig. 4.

3.4. Meanings of nondimensional parameters obtained from linear analysis

In the previous subsection, we conducted a linear analysis for TVC, and demonstrated that the evolution of infinitesimal perturbations is controlled by three nondimensional parameters f, g, and n. In this section, we discuss the physical meanings of f and g.

We examine how the stress τ evolves with time in response to a velocity step. We split the response into two parts; namely a short-term response where a temperature change can be ignored and a long-term response where a temperature change is taken into account.

We first consider the short-term response without a temperature change. By assuming $\delta T_{\mathrm{c}}=0$ in Eq. (21) we get

$$\frac{\mathrm{d}}{\mathrm{d}t}(\delta\tau)=-\frac{\kappa}{h^2}f\delta\tau+\frac{G_{\mathrm{eff}}}{h}\delta V_{\mathrm{w}}. \tag{28}$$

This equation means that $\delta\tau$ evolves with time in response to δV_{w} at an evolution rate of $(\kappa/h^2)f$. In other words, f is the ratio of a timescale of thermal diffusion (h^2/κ) to the stress relaxation time of Maxwell viscoelastic material. Taken together with the assumption of $\delta T_{\mathrm{c}}=0$, the parameter f characterizes the rate of temporal change of τ which takes place instantaneously and/or in the absence of changes in T_{c}.

Eq. (28) also indicates that smaller f slows down the rate of stress reduction due to the viscous deformation. From an analogy of stick–slip behavior of rocks in laboratory experiments, shear instability takes place only when the rate of stress reduction due to viscous deformation is smaller than that due to elastic deformation. Indeed, Fig. 5 shows that the evolution of perturbation is more unstable for smaller f. This is consistent with the results of the linear stability analysis of shear zone formation (Ogawa, 1987).

Next we consider the long-term response including a temperature change. We assume that a new steady state is achieved for a suffciently long time after giving a velocity step ($\exp(\lambda_1 t)$ and $\exp(\lambda_2 t)\to 0$ for $t\to\infty$). By letting $t\to\infty$ in Eq. (23) we obtain,

$$\delta\tau_{(t\to\infty)}=\frac{hG_{\mathrm{eff}}}{\kappa}\delta V_{\mathrm{w}}\frac{1-g}{f(1+g/n)}, \tag{29}$$

or,

$$\left(\frac{\delta\tau}{\delta V_{\mathrm{w}}}\right)_{(t\to\infty)}=\frac{hG_{\mathrm{eff}}}{\kappa}\frac{1-g}{f(1+g/n)}. \tag{30}$$

Note that the denominator in Eq. (30) is always positive. Eq. (30) means that the parameter g deter-

mines the sign of $(\delta\tau/\delta V_w)_{(t\to\infty)}$ and, in other words, determines whether the steady state is potentially stable or not. When $g>1$, the sign of $(\delta\tau/\delta V_w)_{(t\to\infty)}$ is negative ("velocity-weakening") and, hence, an unstable evolution is expected to occur. This is consistent with the results of the linear stability analysis. Indeed, Fig. 5 shows that the regimes U1 and U2 where an unstable evolution occurs take place only when $g>1$, implying that the inequality $g>1$ is necessary for the occurrence of instability. (Note that Eq. (30) can be applied to the rate-dependence of friction only when a steady state is considered. The steady-state deformation is purely viscous (see Eq. (14)), which is consistent with the fact that frictional sliding is inelastic.)

The meaning of the parameter g can be also understood from the viewpoint of the occurrence of thermal instability. Thermal instability takes place when there is a positive feedback in temperature rise; a subtle positive temperature perturbation must cause a further temperature increase. As can be seen from Eq. (22), the condition $g>1$ is necessary for the occurrence of the positive feedback. The two terms δT_c and $\partial(\delta T_c)/\partial t$ have the same sign only when $g>1$. The parameter g is also referred to as Gruntfest number (Gruntfest, 1963), which is defined by the ratio of a timescale of thermal diffusion to that of temperature rise by viscous dissipation. Earlier analytical studies of shear zone formation (e.g. Gruntfest, 1963; Ogawa, 1987) demonstrated that an instability due to shear heating takes place when the Gruntfest number is larger than a threshold value.

We note that the parameter g depends on ambient conditions. In Fig. 6, we show the variation in g depending on T_w and V_w. Fig. 6 clearly shows that g is larger for lower T_w or higher V_w. This feature can be understood from the effects of heating by viscous dissipation. The rate of viscous dissipation becomes higher when the stress and/or the viscous strain rate are higher. A lower T_w yields a higher viscosity and, hence, results in a higher stress and a higher rate of viscous dissipation for a given velocity. A higher V_w, on the other hand, causes a higher rate of viscous strain and, hence, results in a higher rate of viscous dissipation for a given T_w.

The dependence on T_w of g described in Fig. 6 implies that the sign of $(\delta\tau/\delta V_w)_{(t\to\infty)}$ for the steady-state deformation in the present model changes from

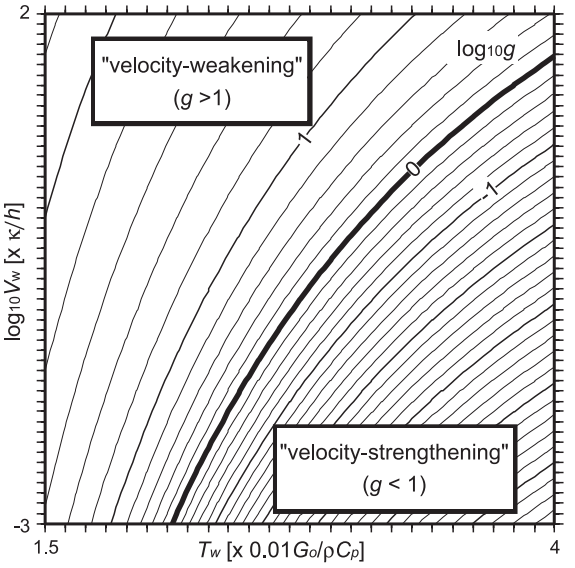

Fig. 6. Variation of the logarithm of nondimensional parameter g depending on T_w and V_w. The values of g is calculated for the set of parameters in Table 1. The thick contour indicates $\log_{10} g=0$, i.e. $g=1$. The units of temperature and velocity are $G/\rho C_p=3.33\times10^4$ K and $\kappa/h=10^{-11}$ m/s, respectively.

negative to positive ("velocity-strengthening") as temperature T_w becomes higher. This feature captures the basic feature of actual rock friction. As demonstrated by rock friction experiments (e.g. Stesky, 1978; Blanpied et al., 1998), frictional slip tends to be stable for a higher ambient temperature. This tendency is qualitatively consistent with the temperature-dependence of g described above.

3.5. Relations between parameters of thermal–viscous coupling and parameters of rate- and state-dependent friction

In the previous sections, we conducted the linear analysis of steady states both for the cases with TVC and with LRSF. The comparison of the results suggests that the evolution of perturbations in TVC is quite similar to that in LRSF. In both cases, the type of evolution is classified into four regimes (see Figs. 2 and 5). Moreover, the evolution becomes more unstable either when the parameter g or β is larger or when f or γ is smaller. The similarity implies that the parameters f and g obtained for TVC can be related with the constitutive parameters appearing in LRSF.

To study the relations between the parameters more clearly, we discuss TVC from a viewpoint of GRSF by Ruina (1983). We examine the shear stress acting in the inner viscous layer. From the assumption of viscous rheology $\dot{\varepsilon}_v = \dot{\varepsilon}_{v(\tau,T_c)}$, the shear stress τ can be written as,

$$\tau = \tau_{(\dot{\varepsilon}_v,T_c)} \equiv F_{tvc(\dot{\varepsilon}_v,T_c)}. \tag{31}$$

In addition, Eq. (12) for the temporal change of T_c can be rewritten as,

$$\frac{dT_c}{dt} = -\frac{\kappa}{h^2}(T_c - T_w) + \frac{1}{\rho C_p}\tau_{(\dot{\varepsilon}_v,T_c)}\dot{\varepsilon}_v \equiv G_{tvc(\dot{\varepsilon}_v,T_c)}. \tag{32}$$

The above two equations mean that TVC is a special case of GRSF, if we regard τ as a frictional force μN, T_c as a state variable Θ, and ε_v as a slip velocity V.

By using F_{tvc} and G_{tvc}, we derive the parameters describing the equation of growth rate λ. From an analogy of Eqs. (3), (4) and (5), we can define a characteristic evolution rate ω' and two nondimensional parameters f' and g' as,

$$\omega' \equiv -G_{tvc,T_c}, \tag{33}$$

$$f' \equiv -G_{eff}\frac{1}{F_{tvc,\dot{\varepsilon}_v}G_{tvc,T_c}}, \tag{34}$$

$$g' \equiv \frac{F_{tvc,T_c}}{F_{tvc,\dot{\varepsilon}_v}}\frac{G_{tvc,\dot{\varepsilon}_v}}{G_{tvc,T_c}}, \tag{35}$$

where the commas in subscripts indicate partial differentiation. The parameter ω' is defined as the rate of change in T_c owing to both conductive cooling and viscous dissipation. The parameter f' is the ratio of the rate of elastic loading by the increase in $\dot{\varepsilon}_v$ ($= G_{eff}\delta\dot{\varepsilon}_v$, where $\delta\dot{\varepsilon}_v$ is a perturbation in $\dot{\varepsilon}_v$) to the rate of the increase in τ directly coming from $\delta\dot{\varepsilon}_v$ ($= \omega' F_{tvc,\dot{\varepsilon}_v}\delta\dot{\varepsilon}_v$). The parameter g' represents the ratio of the rate of decrease in τ due to the increase in $\dot{\varepsilon}_v$ through the change in T_c ($= -F_{tvc,T_c}G_{tvc,\dot{\varepsilon}_v}\delta\dot{\varepsilon}_v$) to the rate of increase in τ directly from the increase in $\dot{\varepsilon}_v$ ($= \omega F_{tvc,\dot{\varepsilon}_v}\delta\dot{\varepsilon}_v$). By using these parameters, the equation of growth rate λ can be written as $\lambda^2 + \omega'(f' + 1 - g')\lambda + (\omega')^2 f' = 0$. In addition, by comparing this equation with Eq. (2), we obtain the correspondence between ω and ω', between β and g', and between γ and f'.

Next we derive the relations between the parameters ω', f' and g' and the parameters f, g, and n defined in Section 3.3. By taking the partial derivatives of F_{tvc} and G_{tvc}, we obtain,

$$\omega' = \frac{\kappa}{h^2} + \frac{1}{\rho C_p}\left(\frac{\partial\tau}{\partial T_c}\right)\dot{\varepsilon}_v = \frac{\kappa}{h^2}\left(1 + \frac{g}{n}\right), \tag{36}$$

$$f' = G_{eff}\left(\frac{\partial\dot{\varepsilon}}{\partial\tau}\right)\omega'^{-1} = f\left(1 + \frac{g}{n}\right)^{-1}, \tag{37}$$

$$g' = \left(\frac{\partial\dot{\varepsilon}_v}{\partial T_c}\right)\frac{1}{\rho C_p}\left[\left(\frac{\partial\dot{\varepsilon}_v}{\partial\tau}\right)^{-1}\dot{\varepsilon}_v + \tau\right]\omega'^{-1} = g\left(1 + \frac{1}{n}\right)\left(1 + \frac{g}{n}\right)^{-1}. \tag{38}$$

By further assuming the correspondence between ω' and ω, between f' and γ, and between g' and β, we can relate the nondimensional parameters f, g, and n with the constitutive parameters appearing in the phenomenological friction law (LRSF) such as Eq. (6).

The differences between the parameters f and f' and between g and g' come from the difference in the timescales assumed in the analysis. The definition of f and g is done with the timescale of conductive cooling (h^2/κ) only, while the definition of f' and g' is with the timescale which incorporates the effects of both conductive cooling and viscous dissipation (see Eq. (36)). Since the latter timescale is defined more naturally from Eq. (32), the parameters f′ and g′ are more appropriate for discussing the relationship between TVC and LRSF. However, the parameters f and g are still useful as a proxy of β and γ. As demonstrated in Eq. (25), the parameters f and g can be used in determining whether a steady state is stable or not against a perturbation (see Eq. (26)).

We also notice that the parameters f and f' and the parameters g and g' become identical if we take the limit of $n \to \infty$. The condition is satisfied when the viscous deformation is significantly small (namely large $\tau_s/\dot{\varepsilon}_s$) and/or when the rate of viscous deformation is highly dependent on stress (namely large $(\partial\dot{\varepsilon}_v/\partial\tau)_{(\tau_s,T_s)}$). Considering the results of laboratory experiments on the creep of crystals and on rock

friction, these two conditions are most likely to be satisfied under some conditions. The first condition is qualitatively consistent with the assumption of LRSF that a frictional slip takes place in a static or quasi-static manner (Dieterich, 1979). The second condition is approximately satisfied for a low-temperature plastic deformation of crystals. For a low-temperature plasticity, crystals deform owing to the glide motion of crystalline dislocations without recovery. When the mobility of dislocations is controlled by a lattice resistance (''Peierls stress''), the rate of deformation becomes highly dependent on stress (Guyot and Dorn, 1967; Frost and Ashby, 1982, Kameyama et al., 1999).

Finally, we should recall a fundamental difference between TVC and LRSF. In TVC, the temporal change in the strength (viscosity) is caused by the conductive cooling and viscous heating, both of which determine the rate of change in T_c. This implies that the growth of perturbations for the case of TVC is controlled by ''characteristic time'' rather than ''characteristic distance'' for the case with LRSF. In LRSF, the characteristic time is determined by the timescale over which a slip distance is equal to d_c at a given slip rate, which means that the characteristic length scale is of primary importance.

4. Discussion and concluding remarks

We developed the idea of the similarity between thermal–viscous coupling (TVC) and frictional slip proposed by Kameyama and Kaneda (2002). By carrying out velocity-stepping tests both numerically and analytically, we found that the stability of steady-state deformation is determined by three nondimensional parameters f, g, and n (see Eqs. (18)–(20)). By applying the theory of generalized rate- and state-dependent friction (Ruina, 1983) to TVC, we obtained the relationship between the nondimensional parameters defined for TVC and the constitutive parameters appearing in the phenomenological form of rate- and state-dependent friction law (LRSF). In addition, from the temperature-dependence of the parameter g we demonstrated that the steady-state deformation of this model is unstable for lower T_w while it is stable for higher T_w. This is consistent with the conjecture that the downdip limit of seismogenic zones is marked by the transition in slip stability due to temperature rise with depth (Scholz, 1990). Although TVC has been applied only to a model of intermediate- or deep-focus earthquakes within subducting slabs (Hobbs and Ord, 1988; Ogawa, 1987), these results might suggest that TVC is also applicable to an estimation of constitutive parameters of slip along seismogenic faults in the shallow portion of the Earth.

In applying the present analysis of TVC to actual faults, uncertainty lies in an estimation of L, the thickness of host rocks surrounding a fault zone. The value of L can be roughly estimated by assuming that L is close to the dimension of the fault surface, because L represents the size of the region where elastic energy is stored. However, uncertainty in L does not affect the condition whether a steady-state deformation is velocity-weakening or velocity-strengthening. Indeed, the parameter g, which determines whether thermal instability occurs or not, is independent of L (see Eq. (19)).

Instead, we should note that the present model assumed a ductile or viscous flow law, under which the dependence on normal stress of shear resistance is ignored. This assumption requires that the entire fault zone deforms in a ductile manner. Thus, the present model can be applicable, to some extent, to the estimation of constitutive parameters near the downdip limit of seismogenic zones of interplate or inland earthquakes, since a ductile deformation is expected to be significant in those regions (Shimamoto, 1985; Iio and Kobayashi, 2003). Owing to the assumptions of flow law, however, the present model cannot be applicable in the brittle friction regime. In the brittle regime, the temporal evolution of frictional resistance is most likely to be controlled by the evolution of the contact state of interfaces (e.g. Bowden and Tabor, 1964; Rabinowicz, 1965; Dieterich and Kilgore, 1994), which is attributed to a viscous creep at contact junctions (e.g. Rice et al., 2001; Nakatani, 2001). In this case, the assumption of the present model is not valid because viscous creep takes place only in very narrow regions. Indeed, the brittle frictional resistance depends on normal stress, which disagrees with a flow law.

In addition to the ductile flow law, the present model is based on several assumptions inappropriate for a model of actual fault slip. First, velocity-weakening is not the only possible mechanism for the

occurrence of unstable slip. Several mechanisms other than thermal–viscous coupling have been proposed as a dominant mechanism for the localization of deformation, or shear instability, in the ductile fields (e.g. Poirier, 1980; Kameyama et al., 1997). Furthermore, a temperature rise does not always decrease the strength of material if the effect of melting is taken into account. High-speed friction experiment at room temperatures (Tsutsumi and Shimamoto, 1997) demonstrated that frictional melting increases the steady-state friction in the velocity-weakening regime.

Nonetheless, an important result of our study is that we obtained one possible estimation of the constitutive parameters of LRSF, especially at depth along seismogenic faults. In most earlier studies of earthquake cycles using the LRSF law (e.g. Tse and Rice, 1986; Stuart, 1988; Kato and Hirasawa, 1997; Kuroki et al., 2002), the distributions of the constitutive parameters must have been assumed a priori, because the values of constitutive parameters are not well understood under the ambient conditions at depth. Hence, further studies on the physical nature of constitutive parameters are necessary, both theoretically and experimentally, in order to thoroughly understand the conditions for the occurrence of unstable seismogenic slip. We speculate that a further improvement of the present approach could lead to a successful estimation of the actual distributions of frictional constitutive parameters along the entire seismogenic faults.

The present approach may be applicable to any irreversible (or inelastic) process other than TVC. If the effect of a certain irreversible process, such as motion of crystalline dislocations or crack growth, is expressed in the form of GRSF, one can define nondimensional parameters similar to f, g and n for TVC, which can be then related to frictional constitutive parameters in LRSF. We thus expect that an extension of present approach may help to estimate the effects of any irreversible process on frictional constitutive relations.

Acknowledgements

I thank Drs. Bruce E. Hobbs, Mitsuhiro Toriumi and Hidemi Tanaka for stimulating discussion and encouragements. I also thank Drs. Naoyuki Kato, Norm Sleep, and an anonymous reviewer for helpful comments which greatly improved the manuscript.

References

Ben-Zion, Y., Rice, J.R., 1995. Slip patterns and earthquake populations along different classes of faults in elastic solids. J. Geophys. Res. 100, 12959–12983.

Blanpied, M.L., Tullis, T.E., Weeks, J.D., 1998. Effects of slip, slip rate, and shear heating on the friction of granite. J. Geophys. Res. 103, 489–511.

Bowden, F.P., Tabor, D., 1964. The Friction and Lubrication of Solids, Part 2. Clarendon, Oxford 544 pp.

Dieterich, J.D., 1979. Modeling of rock friction 1: experimental results and constitutive equation. J. Geophys. Res. 84, 2161–2168.

Dieterich, J.D., Kilgore, B.D., 1994. Direct observation of friction contacts: new insights for state-dependent properties. Pure Appl. Geophys. 143, 283–302.

Frost, H.J., Ashby, M.F., 1982. Deformation-Mechanism Maps; The Plasticity and Creep of Metals and Ceramics. Pergamon, Oxford 168 pp.

Gruntfest, I.J., 1963. Thermal feedback in liquid flow: plane shear at constant stress. Trans. Soc. Rheol. 7, 195–207.

Guyot, P., Dorn, J.E., 1967. A critical review of the Peierls mechanism. Can. J. Phys. 45, 983–1015.

Hobbs, B.E., Ord, A., 1988. Plastic instabilities: implications for the origin of intermediate and deep focus earthquakes. J. Geophys. Res. 93, 10521–10540.

Iio, Y., Kobayashi, Y., 2003. Is the plastic flow uniformly distributed below the seismogenic region? Tectonophysics 364, 43–53.

Kameyama, M., Kaneda, Y., 2002. Thermal–mechanical coupling in shear deformation of viscoelastic material as a model of frictional constitutive relations. Pure Appl. Geophys. 159, 2011–2028.

Kameyama, M., Yuen, D.A., Fujimoto, H., 1997. The interaction of viscous heating with grain-size dependent rheology in the formation of localized slip zones. Geophys. Res. Lett. 24, 2523–2526.

Kameyama, M., Yuen, D.A., Karato, S.-I., 1999. Thermal–mechanical effects of low temperature plasticity (the Peierls mechanism) on the deformation of a viscoelastic shear zone. Earth Planet. Sci. Lett. 168, 159–172.

Karato, S.-I., Paterson, M.S., FitzGerald, J.D., 1986. Rheology of synthetic olivine aggregates: influence of grain size and water. J. Geophys. Res. 91, 8151–8176.

Kato, N., Hirasawa, T., 1997. A numerical study on seismic coupling along subduction zones using a laboratory-derived friction law. Phys. Earth Planet. Inter. 102, 51–68.

Kuroki, H., Ito, H., Yoshida, A., 2002. A three-dimensional simulation of crustal deformation accompanied by subduction in the Tokai region, central Japan. Phys. Earth Planet. Sci. 132, 39–58.

Marone, C., 1998. Laboratory-derived friction laws and their ap-

plication to seismic faulting. Ann. Rev. Earth Planet. Sci. 26, 643–696.

Nakatani, M., 2001. Conceptual and physical clarification of rate and state friction: frictional sliding as a thermally activated rheology. J. Geophys. Res. 106, 13347–13380.

Ogawa, M., 1987. Shear instability in a viscoelastic material as the cause of deep focus earthquakes. J. Geophys. Res. 92, 13801–13810.

Poirier, J.-P., 1980. Shear localization and shear instability in materials in the ductile field. J. Struct. Geol. 2, 135–142.

Rabinowicz, E., 1965. Friction and Wear of Materials. Wiley, New York 244 pp.

Rice, J.R., 1993. Spatio-temporal complexity of slip on a fault. J. Geophys. Res. 98, 9885–9907.

Rice, J.R., Tse, S.T., 1986. Dynamic motion of a single degree of freedom system following a rate and state dependent friction law. J. Geophys. Res. 91, 521–530.

Rice, J.R., Lapusta, N., Ranjith, K., 2001. Rate and state dependent friction and the stability of sliding between elastically deformable solids. J. Mech. Phys. Solids 49, 1865–1898.

Ruina, A., 1983. Slip instability and state variable friction laws. J. Geophys. Res. 88, 10359–10370.

Scholz, C.H., 1990. The Mechanics of Earthquakes and Faulting. Cambridge Univ. Press, New York 439 pp.

Scholz, C.H., 1998. Earthquakes and friction laws. Nature 391, 37–42.

Shimamoto, T., 1985. The origin of large or great thrust-type earthquakes along subducting plate boundaries. Tectonophysics 119, 37–65.

Stesky, R.M., 1978. Mechanisms of high temperature frictional sliding of Westerly Granite. Can. J. Earth Sci. 15, 361–375.

Stuart, W.D., 1988. Forecast model for great earthquakes at the Nankai trough subduction zone. Pure Appl. Geophys. 126, 619–641.

Tse, S.T., Rice, J.R., 1986. Crustal earthquake instability in relation to depth variation of frictional slip properties. J. Geophys. Res. 91, 9452–9472.

Tsutsumi, A., Shimamoto, T., 1997. High-velocity frictional properties of gabbro. Geophys. Res. Lett. 24, 699–702.